

Transport spin polarization of noncollinear antiferromagnetic antiperovskites

Gautam Gurung, Ding-Fu Shao*, and Evgeny Y. Tsymbal†

Department of Physics and Astronomy & Nebraska Center for Materials and Nanoscience,
University of Nebraska, Lincoln, Nebraska 68588-0299, USA

(Received 31 August 2021; accepted 2 December 2021; published 17 December 2021)

Spin-polarized currents play a key role in spintronics. Recently, it has been found that antiferromagnets with a non-spin-degenerate band structure can efficiently spin-polarize electric currents, even though their net magnetization is zero. Among the antiferromagnetic metals with magnetic space group symmetry supporting this functionality, the noncollinear antiferromagnetic antiperovskites $AN\text{Mn}_3$ ($A = \text{Ga, Ni, Sn, or Pt}$) are especially promising. This is due to their high Néel temperatures and a good lattice match to perovskite oxide substrates, offering possibilities of high structural quality heterostructures based on these materials. Here, we investigate the spin polarization of antiferromagnetic $AN\text{Mn}_3$ metals using first-principles density functional theory calculations. We find that the spin polarization of the longitudinal currents in these materials is comparable with that in widely used ferromagnetic metals and thus can be exploited in magnetic tunnel junctions and spin transfer torque devices. Moreover, for certain film growth directions, out-of-plane transverse spin currents with a giant charge-to-spin conversion efficiency can be achieved, implying that the $AN\text{Mn}_3$ antiperovskites can be used as efficient spin sources. These properties make $AN\text{Mn}_3$ compounds promising for application in spintronics.

DOI: 10.1103/PhysRevMaterials.5.124411

Spintronics exploits the spin degree of freedom in electronic devices for information processing and storage [1]. The magnetic order parameter is used as the state variable in these devices, and its detection and manipulation manifest the read and write operations of the stored information. Currents with sizable spin polarization play a central role in the electric performance of such operations used in realistic nanoscale spintronic devices. For example, in magnetic tunnel junctions (MTJs), which are employed in commercial magnetic random-access memories [2], the electrical detection is realized via the tunneling magnetoresistance (TMR) effect signifying a response of the longitudinal spin-polarized charge current to the relative magnetization orientation of the two ferromagnetic electrodes [3–5]. On the other hand, the electric manipulation of magnetization can be achieved via a spin transfer torque driven by a longitudinal spin-polarized charge current [6,7] or via a spin Hall effect [8–10] where a transverse pure spin current is generated by spin-orbit coupling.

Ferromagnetic metals have been widely used in spintronics due to their finite magnetization which can easily spin-polarize electric currents. More recently, it was argued that antiferromagnetic spintronics is more promising, due to antiferromagnets being robust against magnetic perturbations, producing no stray fields, and exhibiting ultrafast spin dynamics [11–13]. Nevertheless, until recently, antiferromagnets have been rarely considered efficient to generate spin-polarized currents. This is because most antiferromagnets exhibit a combined $\hat{T}\hat{O}$ symmetry, where \hat{T} is the time reversal symmetry, and \hat{O} is a crystal symmetry. The $\hat{T}\hat{O}$

symmetry enforces Kramers' spin degeneracy and hence vanishing magnetization. While the antiferromagnetic order may lower the symmetry to support some unconventional spin Hall current useful for spin-orbit torque devices [14], the efficiency of the intrinsic charge-to-spin conversion of antiferromagnets [14–16] does not show obvious advantages compared with those of the widely used nonmagnetic heavy metal spin sources [15–17].

Recently, it was found that the $\hat{T}\hat{O}$ symmetry in antiferromagnets can be broken by the noncollinear magnetic order [18] or noncentrosymmetric arrangement of nonmagnetic atoms [19]. The broken $\hat{T}\hat{O}$ symmetry was shown to result in interesting electronic, magnetic, and transport properties that previously were only known for ferromagnets, such as the anomalous Hall effect [16,18–33], the nonrelativistic Zeeman-like band splitting [34–36], and the unconventional charge-to-spin conversion [37–42]. The emergence of electric currents with sizable spin polarization is particularly exciting due to the possible use of these currents and the antiferromagnets generating them in spintronic devices [43–45].

Among the antiferromagnetic material candidates exhibiting the required magnetic space group symmetry to produce spin-polarized currents, Mn-based antiperovskite nitrides $AN\text{Mn}_3$ ($A = \text{Ga, Ni, Sn, or Pt}$) [46] have a few advantages. These antiferromagnetic metals have sufficiently high Néel temperatures, often about room temperature [46,47]. Also, their crystal structures match well to those of the widely used perovskite oxides, which allows the realization of high-quality epitaxial heterostructures for device fabrication [14,48].

In this paper, based on first-principles density functional theory calculations, we explore the spin polarization of $AN\text{Mn}_3$ ($A = \text{Ga, Ni, Sn, or Pt}$) antiferromagnetic metals [49–64]. We find that the longitudinal charge currents passing through $AN\text{Mn}_3$ can have a sizable spin polarization, which

*dfshao@unl.edu

†tsymbal@unl.edu

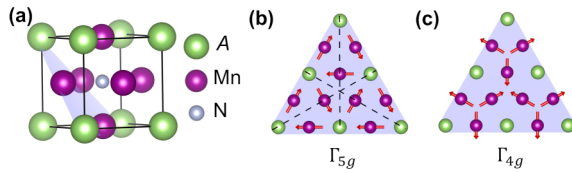


FIG. 1. (a) Atomic structure of antiperovskite $ANMn_3$. (b) and (c) The noncollinear alignment of Mn moments in the (111) plane for the antiferromagnetic (b) Γ_{5g} and (c) Γ_{4g} phases. Red arrows denote magnetic moments, and dashed black lines indicate mirror planes $\hat{M}_{0\bar{1}\bar{1}}$, $\hat{M}_{1\bar{0}\bar{1}}$, and $\hat{M}_{\bar{1}\bar{1}0}$ for the Γ_{5g} phase.

allows using antiperovskites in MTJs and spin transfer torque devices. Moreover, we show that the out-of-plane transverse spin currents with giant charge-to-spin conversion efficiencies can be achieved by controlling the film growth direction. These properties make $ANMn_3$ compounds promising for application in spintronics.

Figure 1(a) shows the crystal structure of the antiperovskite $ANMn_3$, which is like that of a perovskite except for the cation and the anion having swapped positions [Fig. 1(a)]. This structure hosts a frustrated Kagomé lattice in the (111) plane that favors noncollinear alignment of the antiferromagnetically coupled magnetic moments [46]. The antiperovskites exhibit interesting properties, such as magnetovolume [47], barocaloric [65], piezomagnetic [61,62,66], magnetoelectric [63,67], anomalous Hall [23–28], and unconventional spin Hall [14] effects. One of the most common noncollinear antiferromagnetic orders in $ANMn_3$ is Γ_{5g} (typical for $GaN Mn_3$), where the Mn magnetic moments form a chiral configuration with the 120° angle between each other within the (111) plane [Fig. 1(b)] [46,60]. Here, Γ_{5g} is a compensated antiferromagnetic phase due to three mirror planes $\hat{M}_{0\bar{1}\bar{1}}$, $\hat{M}_{1\bar{0}\bar{1}}$, or $\hat{M}_{\bar{1}\bar{1}0}$ perpendicular to the (111) plane in the magnetic space group $R\bar{3}m$ which prohibit the net magnetization. Another common noncollinear antiferromagnetic phase is Γ_{4g} , which can be obtained from the Γ_{5g} phase by rotating all magnetic moments about the [111] axis by 90° [Fig. 1(c)] [46]. The mirror symmetries are broken in the Γ_{4g} phase so that the corresponding magnetic space group $R\bar{3}m'$ allows an uncompensated magnetization (though very small) and the anomalous Hall effect [23,68].

We find that the magnetic group symmetries of both Γ_{5g} and Γ_{4g} phases support sizable longitudinal and transverse spin currents. In the diffusive transport regime, the spin conductivity has two contributions [8,37]:

$$\sigma_{ij}^k = -\frac{e\hbar}{\pi} \int \frac{d^3\vec{k}}{(2\pi)^3} \times \sum_{n,m} \frac{\Gamma^2 \text{Re}(\langle n\vec{k}|J_i^k|m\vec{k}\rangle \langle m\vec{k}|v_j|n\vec{k}\rangle)}{[(E_F - E_{n\vec{k}})^2 + \Gamma^2][(E_F - E_{m\vec{k}})^2 + \Gamma^2]}, \quad (1)$$

and

$$\sigma_{ij}^k = -\frac{2e}{\hbar} \int \frac{d^3\vec{k}}{(2\pi)^3} \sum_{m \neq n} \frac{\text{Im}(\langle n\vec{k}|J_i^k|m\vec{k}\rangle \langle m\vec{k}|v_j|n\vec{k}\rangle)}{(E_{n\vec{k}} - E_{m\vec{k}})^2}. \quad (2)$$

Here, $J_i^k = \frac{1}{2}\{v_i, s_k\}$ is the spin current operator, Γ is the scattering rate in a constant relaxation time approximation, $f_{n\vec{k}}$

is the Fermi-Dirac distribution function for band n and wave vector \vec{k} , v_i and s_k are velocity and spin operators, respectively, and i , j , and k are the spin-current, charge-current, and spin-polarization directions, respectively. The spin conductivity σ_{ij}^k given by Eq. (1) is the odd Fermi surface property under time reversal symmetry (\hat{T} -odd). As a result, this contribution is allowed only for ferromagnetic and some antiferromagnetic metals without \hat{T} or $\hat{T}\hat{O}$ symmetries, such as noncollinear antiferromagnetic $ANMn_3$. In these materials, the Fermi surface is intrinsically spin textured, resulting in spin-polarized currents even in the absence of spin-orbit coupling. This leads to finite nonrelativistic components of the \hat{T} -odd spin conductivity tensor. Spin-orbit coupling alters the spin texture and hence the spin conductivity tensor. However, due to the electronic structure of $ANMn_3$ at the Fermi energy (E_F) being majorly controlled by the Mn atoms which do not produce strong spin-orbit coupling, these changes are not expected to be significant (note though that the spin-orbit coupling makes some σ_{ij}^k components finite, which were zero in its absence).

In contrast to the \hat{T} -odd σ_{ij}^k , the spin conductivity tensor given by Eq. (2) is determined by the interband contributions that are even under time reversal symmetry (\hat{T} -even). As a result, nonvanishing \hat{T} -even σ_{ij}^k components can only appear in the presence of spin-orbit coupling. Therefore, these relativistic components are expected to be small compared with the nonrelativistic components of the \hat{T} -odd σ_{ij}^k (see Supplemental Material [49]). Thus, in the following, we focus only on the \hat{T} -odd spin conductivity of $ANMn_3$.

Table I displays the \hat{T} -odd σ_{ij}^k of $ANMn_3$ according to the magnetic space group symmetry of the crystal. For a (001)-stacked $ANMn_3$ with the x , y , and z axes aligned along the [100], [010], and [001] crystal directions, there are four independent tensor components (denoted by a – d) in the Γ_{5g} phase. These include the off-diagonal tensor components σ_{ij}^k ($i \neq j$) which determine the transverse spin current generated by a longitudinal charge current and are related to the magnetic spin Hall effect proposed recently [37–40]. However, these off-diagonal components are relativistic in nature and are nonzero only in the presence of spin-orbit coupling. Therefore, these relativistic contributions to spin conductivity are not expected to be large due to the weak spin-orbit coupling in $ANMn_3$.

There are also nonrelativistic diagonal components of the spin conductivity tensor σ_{jj}^k ($k \neq j$). These components determine a longitudinal spin current carrying a transverse spin polarization generated by a longitudinal charge current. These diagonal components are nonzero even in the absence of spin-orbit coupling and hence are expected to be large. This implies that a longitudinal spin-polarized charge current can be produced in the compensated antiferromagnetic Γ_{5g} phase.

To obtain a more intuitive understanding of why the longitudinal charge current is spin-polarized, we use $GaN Mn_3$ as a representative example and explore its momentum-dependent spin texture. Due to the broken \hat{T} symmetry in antiferromagnetic $GaN Mn_3$, the spin degeneracy is lifted, and hence, the spin expectation values $\langle s \rangle$ are finite. Since the \hat{T} -odd spin conductivity is a purely Fermi surface property [see Eq. (1)], it is the spin texture at the Fermi surface that matters. Figure 2(a) shows the calculated expectation values of the x , y , and z components of the spin at the Fermi surface of $GaN Mn_3$ in

TABLE I. \hat{T} -odd spin conductivity tensors for the Γ_{5g} and Γ_{4g} phases of ANMn_3 . The x , y , and z axes are set along the [100], [010], and [001] directions for a (001)-stacked film and along the [$\bar{1}10$], [001], and [110] directions for a (110)-stacked film. The matrix elements in the parentheses only appear in the presence of spin-orbit coupling.

	$\sigma^x = \begin{bmatrix} \sigma_{xx}^x & \sigma_{xy}^x & \sigma_{xz}^x \\ \sigma_{yx}^x & \sigma_{yy}^x & \sigma_{yz}^x \\ \sigma_{zx}^x & \sigma_{zy}^x & \sigma_{zz}^x \end{bmatrix}$	$\sigma^y = \begin{bmatrix} \sigma_{xx}^y & \sigma_{xy}^y & \sigma_{xz}^y \\ \sigma_{yx}^y & \sigma_{yy}^y & \sigma_{yz}^y \\ \sigma_{zx}^y & \sigma_{zy}^y & \sigma_{zz}^y \end{bmatrix}$	$\sigma^z = \begin{bmatrix} \sigma_{xx}^z & \sigma_{xy}^z & \sigma_{xz}^z \\ \sigma_{yx}^z & \sigma_{yy}^z & \sigma_{yz}^z \\ \sigma_{zx}^z & \sigma_{zy}^z & \sigma_{zz}^z \end{bmatrix}$
Γ_{5g} ANMn ₃ (001)	$\begin{bmatrix} 0 & (-a) & (a) \\ (b) & -c & (-d) \\ (-b) & (d) & c \end{bmatrix}$	$\begin{bmatrix} c & (-b) & (d) \\ (a) & 0 & (-a) \\ (-d) & (b) & -c \end{bmatrix}$	$\begin{bmatrix} -c & (-d) & (b) \\ (d) & c & (-b) \\ (-a) & (a) & 0 \end{bmatrix}$
	$\begin{bmatrix} E & (A) & (A) \\ (B) & C & (D) \\ (B) & (D) & C \end{bmatrix}$	$\begin{bmatrix} C & (B) & (D) \\ (A) & E & (A) \\ (D) & (B) & C \end{bmatrix}$	$\begin{bmatrix} C & (D) & (B) \\ (D) & C & (B) \\ (A) & (A) & E \end{bmatrix}$
Γ_{5g} ANMn ₃ (110)	$\begin{bmatrix} \frac{-a+b+c}{\sqrt{2}} & 0 & 0 \\ 0 & -\sqrt{2}c & (b-d) \\ 0 & (-a+d) & \frac{a-b+c}{\sqrt{2}} \end{bmatrix}$	$\begin{bmatrix} 0 & (-\sqrt{2}b) & c+d \\ (\sqrt{2}a) & 0 & 0 \\ c-d & 0 & 0 \end{bmatrix}$	$\begin{bmatrix} 0 & (-a-d) & \frac{a+b-c}{\sqrt{2}} \\ (b+d) & 0 & 0 \\ \frac{-a+b+c}{\sqrt{2}} & 0 & 0 \end{bmatrix}$
	$\begin{bmatrix} 0 & (A-D) & \frac{A-B-C+E}{\sqrt{2}} \\ (B-D) & 0 & 0 \\ \frac{-A+B-C+E}{\sqrt{2}} & 0 & 0 \end{bmatrix}$	$\begin{bmatrix} C-D & 0 & 0 \\ 0 & E & (\sqrt{2}A) \\ 0 & (\sqrt{2}B) & C+D \end{bmatrix}$	$\begin{bmatrix} \frac{-A-B+C+E}{\sqrt{2}} & 0 & 0 \\ 0 & \sqrt{2}C & (B+D) \\ 0 & (A+D) & \frac{A+B+C+E}{\sqrt{2}} \end{bmatrix}$

the Γ_{5g} phase, indicating a rather intricate distribution. The same spin texture, but within the (110) plane, is displayed in Fig. 2(b) and enlarged in Fig. 2(c) to focus on the Fermi pocket at the center of the Brillouin zone. These spin textures can make the electric currents flowing along certain crystallographic directions of GaNMn₃ spin polarized.

To demonstrate this, we consider symmetry transformations of the spin texture within this Fermi pocket. The inversion-symmetric fragments of the Fermi pocket have the same spin expectation values since the inversion symmetry \hat{P} does not change the spin:

$$\hat{P}(k_{110}, k_{\bar{1}10}, k_{001}) = (-k_{110}, -k_{\bar{1}10}, -k_{001}),$$

$$\hat{P}(\langle s_{110} \rangle, \langle s_{\bar{1}10} \rangle, \langle s_{001} \rangle) = (\langle s_{110} \rangle, \langle s_{\bar{1}10} \rangle, \langle s_{001} \rangle). \quad (3)$$

Further, the spin expectation values for the wave vectors being symmetric with respect to the $\hat{M}_{\bar{1}10}$ mirror plane have

the same $\langle s_{\bar{1}10} \rangle$ components but opposite $\langle s_{001} \rangle$ and $\langle s_{110} \rangle$ components. This is due to the mirror symmetry operation conserving the spin component normal to the mirror plane but flipping the spin component parallel to it:

$$\hat{M}_{\bar{1}10}(k_{110}, k_{\bar{1}10}, k_{001}) = (k_{110}, -k_{\bar{1}10}, k_{001}),$$

$$\hat{M}_{\bar{1}10}(\langle s_{110} \rangle, \langle s_{\bar{1}10} \rangle, \langle s_{001} \rangle) = (-\langle s_{110} \rangle, \langle s_{\bar{1}10} \rangle, -\langle s_{001} \rangle). \quad (4)$$

As a result, the longitudinal electric current parallel to the [$\bar{1}10$] plane, such as the current along the [001] direction shown in Fig. 2(c), is polarized by this spin texture. The associated spin current J_c has a finite $\langle s_{\bar{1}10} \rangle$ component but zero $\langle s_{110} \rangle$ and $\langle s_{001} \rangle$ components since only $\langle s_{\bar{1}10} \rangle$ is even with respect to $\hat{M}_{\bar{1}10}$. This implies finite matrix elements of the longitudinal spin conductivity tensor $\sigma_{zz}^x = -\sigma_{zz}^y = c$, as shown in Table I for ANMn₃ in the Γ_{5g} phase.

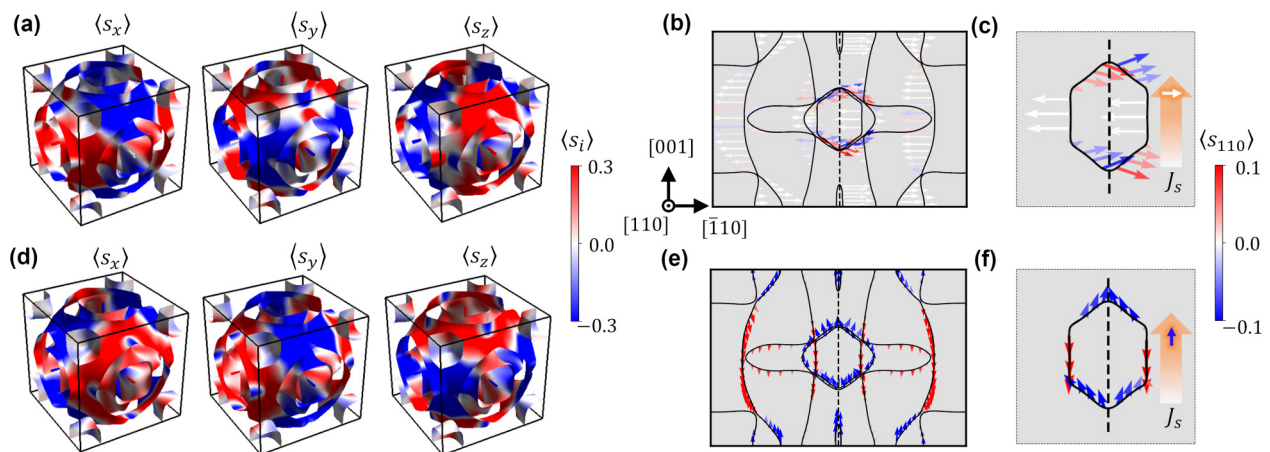


FIG. 2. (a) The spin-projected Fermi surface of GaNMn₃ in the Γ_{5g} phase. (b) The (110) plane cut of the Fermi surfaces shown in (a), where the solid lines denote the Fermi surface, the colored arrows denote the spin textures, and the dashed line denotes the $M_{\bar{1}10}$ mirror plane. (c) The zoomed plot of (b) showing only the central Fermi pocket. (d)–(f) The same in (a)–(c) for GaNMn₃ in the Γ_{4g} phase.

TABLE II. Charge-to-spin conversion efficiency $\Phi(\sigma_{ij}^k) = \frac{2e}{\hbar} \sigma_{ij}^k / \sigma_{jj}$ (in percent) in antiperovskite $AN\text{Mn}_3$ ($A = \text{Ga, Ni, Sn, or Pt}$) in Γ_{5g} and Γ_{4g} phases for (001)- and (110)-stacked films. Calculations were performed in the presence of spin-orbit coupling for $\Gamma = 0.05$ eV. The x , y , and z are set along [100], [010], and [001] directions for (001)-stacked film and along [$\bar{1}10$], [001], and [110] directions for a (110)-stacked film.

	Γ_{5g}				Γ_{4g}				
	GaNMn ₃	NiNMn ₃	SnNMn ₃	PtNMn ₃	GaNMn ₃	NiNMn ₃	SnNMn ₃	PtNMn ₃	
ANMn ₃ (001)	$\Phi(\sigma_{zz}^x)$	-20.7	13.3	-27.0	14.2	-12.3	7.7	-16.0	10.2
	$\Phi(\sigma_{zz}^z)$	0.0	0.0	0.0	0.0	24.4	-15.1	31.2	-18.1
	$\Phi(\sigma_{zx}^x)$	-0.4	-0.7	-0.7	-3.4	-0.1	-0.3	0.6	-1.8
	$\Phi(\sigma_{zx}^y)$	-0.3	-0.4	-0.6	-0.01	-0.8	-0.3	-0.4	-3.8
	$\Phi(\sigma_{zx}^z)$	0.1	0.5	-0.1	1.0	-0.3	-0.2	0.3	-0.1
ANMn ₃ (110)	$\Phi(\sigma_{zz}^x)$	-15.0	8.6	-19.5	6.9	0.0	0.0	0.0	0.0
	$\Phi(\sigma_{zz}^z)$	0.0	0.0	0.0	0.0	8.3	-5.6	11.4	-6.9
	$\Phi(\sigma_{zx}^x)$	0.0	0.0	0.0	0.0	26.1	-16.2	33.6	-21.2
	$\Phi(\sigma_{zx}^y)$	-21.0	12.9	-27.6	14.2	0.0	0.0	0.0	0.0
	$\Phi(\sigma_{zx}^z)$	14.4	-9.5	18.5	-11.7	0.0	0.0	0.0	0.0

In contrast to the Γ_{5g} phase, the Γ_{4g} phase of $AN\text{Mn}_3$ has five independent components (denoted by $A-E$) of the \hat{T} -odd spin conductivity tensor for a (001)-stacked $AN\text{Mn}_3$. We find that both the diagonal components with spin polarization normal to the charge current direction $\sigma_{jj}^k = C$ ($k \neq j$) and those parallel to it $\sigma_{jj}^j = E$ do not vanish in the absence of spin-orbit coupling. This can be illustratively understood by analyzing the spin-projected Fermi surfaces of the Γ_{4g} GaNMn₃ [Figs. 2(d)-2(f)]. The spin textures in the Γ_{4g} phase are very different from those in the Γ_{5g} phase due to different magnetic space group symmetry. The mirror $\hat{M}_{\bar{1}10}$ plane is broken in the Γ_{4g} phase, while a combined $\hat{T}\hat{M}_{\bar{1}10}$ symmetry is preserved, which transforms the wave vector and the spin as follows:

$$\hat{T}\hat{M}_{\bar{1}10}(k_{110}, k_{\bar{1}10}, k_{001}) = (-k_{110}, k_{\bar{1}10}, -k_{001}),$$

$$\hat{T}\hat{M}_{\bar{1}10}(\langle s_{110} \rangle, \langle s_{\bar{1}10} \rangle, \langle s_{001} \rangle) = (\langle s_{110} \rangle, -\langle s_{\bar{1}10} \rangle, \langle s_{001} \rangle). \quad (5)$$

This symmetry together with inversion symmetry \hat{P} [Eq. (3)] implies that $\langle s_{\bar{1}10} \rangle$ is antisymmetric and $\langle s_{110} \rangle$ and $\langle s_{001} \rangle$ are symmetric with respect to the $(\bar{1}10)$ plane. Therefore, a longitudinal electric current parallel to the $(\bar{1}10)$ plane, such as that along the [001] direction, becomes spin polarized with finite $\langle s_{110} \rangle$ and $\langle s_{001} \rangle$ components and a zero $\langle s_{\bar{1}10} \rangle$ component. This implies finite longitudinal spin conductivities $\sigma_{zz}^x = \sigma_{zz}^y = C$ and $\sigma_{zz}^z = E$, as shown in Table I.

The efficiency of the \hat{T} -odd spin current generation can be estimated by calculating a percentage spin conductivity ratio $\Phi(\sigma_{ij}^k) = \frac{2e}{\hbar} \sigma_{ij}^k / \sigma_{jj}$. Here, σ_{jj} is a conductivity of the longitudinal charge current J_c used to generate the spin current J_s with conductivity σ_{ij}^k , which can be calculated by replacing the spin current operator J_i^k in Eq. (1) by the charge current operator $J_i = -ev_i$. Here, $\Phi(\sigma_{ij}^k)$ serves as a figure of merit for the performance of realistic spintronic devices. Specifically, $\Phi(\sigma_{zx}^k)$ represents the spin Hall angle in spin-torque devices with current-in-plane (CIP) geometry, where an out-of-plane spin current is generated by an in-plane charge current. Similarly, $\Phi(\sigma_{zz}^k)$ measures the degree of spin polarization for an out-of-plane charge current in devices

with current-perpendicular-to-plane (CPP) geometry, such as MTJs.

We calculate $\Phi(\sigma_{ij}^k)$ for $AN\text{Mn}_3$ ($A = \text{Ga, Ni, Sn, or Pt}$) compounds assuming they are stacked in the (001) plane. Table II shows the calculated results for $\Gamma = 0.05$ eV, which provides realistic conductivity σ_{zz} of the compounds. For the longitudinal spin conductivity, we find that $\Phi(\sigma_{zz}^i)$ is sizable for all $AN\text{Mn}_3$ antiferromagnets we investigated. Specifically, we obtain $\Phi(\sigma_{zz}^x) = -20.7\%$ for GaNMn₃, which exhibits a Γ_{5g} ground state, and $\Phi(\sigma_{zz}^x) = -16.0\%$ and $\Phi(\sigma_{zz}^z) = 31.2\%$ for SnNMn₃, which has a high-temperature Γ_{4g} state. These sizable spin polarizations of the longitudinal current in antiferromagnetic antiperovskites are comparable with those in ferromagnetic metals, such as Fe, Co, and Ni [69–71], indicating their potential for spintronic applications, such as antiferromagnetic tunnel junctions discussed below. We note that our results are robust with respect to disorder scattering, as follows from our calculations of $\Phi(\sigma_{zz}^k)$ as a function of Γ shown in the Supplemental Material Fig. S1 [49].

On the contrary, the transverse spin conductivity ratio $\Phi(\sigma_{zx}^k)$ is negligible for $AN\text{Mn}_3$ (001) (Table II). This is understandable since the nonrelativistic spin texture does not contribute to σ_{zx}^k , and the effect appears entirely due to small spin-orbit coupling. However, although $AN\text{Mn}_3$ is not efficient for generating transverse spin currents in (001)-stacked films, it can form a good spin current source for spin-torque devices by engineering the $AN\text{Mn}_3$ growth direction. The related spin conductivity tensors for a film with different orientation can be obtained by applying transformation

$$\sigma_{i'j'}^k = \sum_{k,i,j} R_{k'k} R_{i'i} R_{j'j} \sigma_{ij}^k, \quad (6)$$

where σ_{ij}^k is the spin conductivity for a (001)-stacked film with coordinate system (x, y, z) , $\sigma_{i'j'}^k$ is the spin conductivity of a film with coordinate system (x', y', z') , R is the rotation matrix to transform the coordinate system (x, y, z) to (x', y', z') . A nonrelativistic spin texture contribution to $\Phi(\sigma_{zx}^k)$ may be allowed by the magnetic-space group symmetry after the rotation transformation.

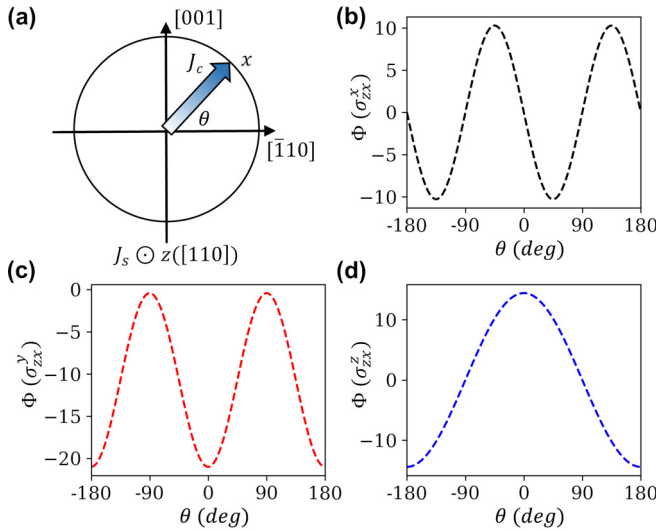


FIG. 3. (a) The schematic of charge-to-spin conversion in an ANMn_3 (110) film. An out-of-plane spin current J_s along the [110] (z) direction is generated by applying an in-plane longitudinal charge current J_c along the x direction, which is away from the [1̄10] direction by the angle θ . (b)–(d) Charge-to-spin conversion efficiency $\Phi(\sigma_{zx}^k)$ as a function of the longitudinal charge current direction for GaNMn_3 (110)-stacked films in the Γ_{5g} phase.

As an example, Table I shows the spin conductivity tensor for ANMn_3 (110) in the Γ_{5g} and Γ_{4g} phases. It is seen that, when the charge current direction (x) is along the [1̄10] direction, finite σ_{zx}^y and σ_{zx}^z appear in the Γ_{5g} phase, and a finite σ_{zx}^x appears in the Γ_{4g} phase, even in the absence of spin-orbit coupling. Table II shows calculated $\Phi(\sigma_{zx}^k)$ for ANMn_3 ($A = \text{Ga, Ni, Sn, or Pt}$) (110) films. For the Γ_{5g} ground state in GaNMn_3 , we find large $\Phi(\sigma_{zx}^y) = -21.0\%$ and $\Phi(\sigma_{zx}^z) = 14.4\%$, which are comparable or even larger than these for the reported spin Hall angle in widely used spin source materials such as Pt [72–74].

Moreover, the transverse σ_{zx}^x component in the Γ_{5g} phase can be engineered by tilting the in-plane longitudinal current direction x from [110] by an angle θ [Fig. 3(a)]. In this case, the σ_{zx}^k components are functions of θ as follows:

$$\begin{aligned} \sigma_{zx}^x &= \frac{-a + c}{2} \sin 2\theta, \\ \sigma_{zx}^y &= \frac{1}{2}(a + c - 2d) - \frac{1}{2}(a - c) \cos 2\theta, \\ \sigma_{zx}^z &= -\frac{a + b + c}{\sqrt{2}} \cos \theta. \end{aligned} \quad (6)$$

Figures 3(b)–3(d) show the respective variations of σ_{zx}^k as functions of θ for GaNMn_3 (110). Similar angular dependences of σ_{zx}^k for the ground states of NiNMn_3 , SnNMn_3 , and PtNMn_3 (110) films can be found in Supplemental Material [49].

The predicted efficient generation of the longitudinal and transverse currents with sizable spin polarization allows promising spintronic devices based on noncollinear antiferromagnetic ANMn_3 . Here, we propose two types of spintronic devices, as shown in Fig. 4. The first one is an antiferromagnetic

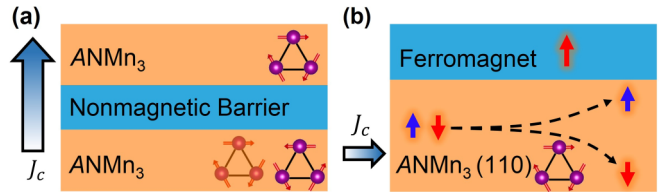


FIG. 4. (a) The schematic of an antiferromagnetic tunnel junction using ANMn_3 as the electrodes, where the transport of the out-of-plane longitudinal spin-polarized current is controlled by the relative orientation of the magnetic moments between two ANMn_3 layers. (b) The schematic of a spin-torque device with current-in-plane (CIP) geometry. An in-plane charge current passes through the ANMn_3 (110) layer and generates an out-of-plane spin current carrying sizable spin polarization collinear to the spin current direction. This spin current can exert a torque on the perpendicular magnetization in the top ferromagnetic layer for an efficient switching.

tunnel junction [37], where the two ANMn_3 electrodes are separated by an insulating nonmagnetic layer [Fig. 4(a)]. The CPP longitudinal spin-polarized current is controlled by the relative orientation of the magnetic order parameters in the ANMn_3 reference and free layers. Due to a large spin polarization of the longitudinal current, the TMR effect is expected to be sizable and hence can be used to efficiently detect the magnetic order parameter in ANMn_3 . The spin-polarized current can be also used to generate the spin-transfer torque for switching ANMn_3 [68,75–77].

The second spintronic device is a CIP spin-torque device, where an ANMn_3 (110) layer is used as a spin source to generate an out-of-plane spin current which enters the top ferromagnetic layer and exerts a torque on its magnetization [Fig. 4(b)]. Since the ANMn_3 (110) layer exhibits large $\Phi(\sigma_{zx}^z)$, the spin current can carry sizable spin component collinear to the spin current direction, which is necessary for switching a ferromagnet with perpendicular anisotropy required for high-density spintronic devices.

We note that the symmetries of bulk antiperovskites are lowered at the interfaces of such devices, which may affect spin-dependent transport properties such as the TMR and spin-transfer torque. It was found, however, that in realistic antiferromagnet/nonmagnet systems, these effects were not essential for the device performance [11,78,79]. We expect therefore that the predicted bulk properties would largely control functional properties of the device structures based on antiferromagnetic antiperovskites.

In conclusion, based on first-principles density functional theory calculations, we have predicted that the noncollinear antiferromagnetic antiperovskites ANMn_3 ($A = \text{Ga, Ni, Sn, or Pt}$) support electric currents with sizable spin polarization. We found that the calculated spin polarization of the longitudinal currents can be comparable with that in widely used ferromagnetic metals, which makes the antiperovskites promising for using in antiferromagnetic tunnel junction and spin transfer torque devices. Furthermore, we demonstrated that by controlling the film growth direction, the out-of-plane transverse spin currents with sizable charge-to-spin conversion efficiencies can be achieved, which implies that the ANMn_3 compounds can serve as effective spin source materials. These properties

make noncollinear antiferromagnetic antiperovskites promising for realistic applications in spintronics.

This paper was supported by the Office of Naval Research (Grant No. N00014-20-1-2844) and by the National Science

Foundation through EPSCoR RII Track-00001 (Award No. OIA-2044049) program. Computations were performed at the University of Nebraska Holland Computing Center. The figures were created using VESTA [57], FERMISURFER [58], and MATPLOTLIB.

[1] E. Y. Tsymbal and I. Žutić, Eds., *Spintronics Handbook: Spin Transport and Magnetism*, 2nd ed. (Taylor & Francis Group, Boca Raton, 2019).

[2] A. V. Khvalkovskiy, D. Apalkov, S. Watts, R. Chepulskii, R. S. Beach, A. Ong, X. Tang, A. Driskill-Smith, W. H. Butler, P. B. Visscher, D. Lottis, E. Chen, V. Nikitin, and M. Krounbi, Basic principles of STT-MRAM cell operation in memory arrays, *J. Phys. D* **46**, 074001 (2013).

[3] M. Julliere, Tunneling between ferromagnetic films, *Phys. Lett. A* **54**, 225 (1975).

[4] J. S. Moodera, L. R. Kinder, T. M. Wong, and R. Meservey, Large Magnetoresistance at Room Temperature in Ferromagnetic Thin Film Tunnel Junctions, *Phys. Rev. Lett.* **74**, 3273 (1995).

[5] E. Y. Tsymbal, O. N. Mryasov, and P. R. LeClair, Spin-dependent tunneling in magnetic tunnel junctions, *J. Phys.: Condens. Matter* **15**, R109 (2003).

[6] J. C. Slonczewski, Conductance and exchange coupling of two ferromagnets separated by a tunneling barrier, *Phys. Rev. B* **39**, 6995 (1989).

[7] D. Ralph and M. Stiles, Spin transfer torques, *J. Magn. Magn. Mater.* **320**, 1190 (2008).

[8] J. Sinova, S. O. Valenzuela, J. Wunderlich, C. H. Back, and T. Jungwirth, Spin Hall effects, *Rev. Mod. Phys.* **87**, 1213 (2015).

[9] I. M. Miron, K. Garello, G. Gaudin, P.-J. Zermatten, M. V. Costache, S. Auffret, S. Bandiera, B. Rodmacq, A. Schuhl, and P. Gambardella, Perpendicular switching of a single ferromagnetic layer induced by in-plane current injection, *Nature (London)* **476**, 189 (2011).

[10] L. Liu, C.-F. Pai, Y. Li, H. W. Tseng, D. C. Ralph, and R. A. Buhrman, Spin-torque switching with the giant spin Hall effect of tantalum, *Science* **336**, 555 (2012).

[11] V. Baltz, A. Manchon, M. Tsoi, T. Moriyama, T. Ono, and Y. Tserkovnyak, Antiferromagnetic spintronics, *Rev. Mod. Phys.* **90**, 015005 (2018).

[12] T. Jungwirth, X. Marti, P. Wadley, and J. Wunderlich, Antiferromagnetic spintronics, *Nat. Nanotechnol.* **11**, 231 (2016).

[13] T. Jungwirth, J. Sinova, A. Manchon, X. Marti, J. Wunderlich, and C. Felser, The multiple directions of antiferromagnetic spintronics, *Nat. Phys.* **14**, 200 (2018).

[14] T. Nan, C. X. Quintela, J. Irwin, G. Gurung, D. -F. Shao, J. Gibbons, N. Campbell, K. Song, S. Y. Choi, L. Guo, R. D. Johnson, P. Manuel, R. V. Chopdekar, I. Hallsteinsen, T. Tybell, P. J. Ryan, J. W. Kim, Y. S. Choi, P. G. Radaelli, D. C. Ralph *et al.*, Controlling spin current polarization through non-collinear antiferromagnetism, *Nat. Commun.* **11**, 4671 (2020).

[15] F. Freimuth, S. Blügel, and Y. Mokrousov, Anisotropic Spin Hall Effect from First Principles, *Phys. Rev. Lett.* **105**, 246602 (2010).

[16] Y. Zhang, Y. Sun, H. Yang, J. Železný, S. P. P. Parkin, C. Felser, and B. Yan, Strong anisotropic anomalous Hall effect and spin Hall effect in the chiral antiferromagnetic compounds Mn_3X ($X = Ge, Sn, Ga, Ir, Rh$, and Pt), *Phys. Rev. B* **95**, 075128 (2017).

[17] G. Y. Guo, S. Murakami, T.-W. Chen, and N. Nagaosa, Intrinsic Spin Hall Effect in Platinum: First-Principles Calculations, *Phys. Rev. Lett.* **100**, 096401 (2008).

[18] H. Chen, Q. Niu, and A. H. MacDonald, Anomalous Hall Effect Arising from Noncollinear Antiferromagnetism, *Phys. Rev. Lett.* **112**, 017205 (2014).

[19] L. Šmejkal, R. González-Hernández, T. Jungwirth, and J. Sinova, Crystal time-reversal symmetry breaking and spontaneous Hall effect in collinear antiferromagnets, *Sci. Adv.* **6**, eaaz8809 (2020).

[20] J. Kübler and C. Felser, Non-collinear antiferromagnets and the anomalous Hall effect, *Europhys. Lett.* **108**, 67001 (2014).

[21] S. Nakatsuji, N. Kiyohara, and T. Higo, Large anomalous Hall effect in a non-collinear antiferromagnet at room temperature, *Nature (London)* **527**, 212 (2015).

[22] A. K. Nayak, J. E. Fischer, Y. Sun, B. Yan, J. Karel, A. C. Komarek, C. Shekhar, N. Kumar, W. Schnelle, J. Kübler, C. Felser, and S. P. P. Parkin, Large anomalous Hall effect driven by a nonvanishing Berry curvature in the noncollinear antiferromagnet Mn_3Ge , *Sci. Adv.* **2**, e1501870 (2016).

[23] G. Gurung, D.-F. Shao, T. R. Paudel, and E. Y. Tsymbal, Anomalous Hall conductivity of non-collinear magnetic antiperovskites, *Phys. Rev. Materials* **3**, 044409 (2019).

[24] D. Boldrin, I. Samarthakis, J. Zemen, A. Mihai, B. Zou, B. Esser, D. McComb, P. Petrov, H. Zhang, and L. F. Cohen, The anomalous Hall effect in non-collinear antiferromagnetic Mn_3NiN thin films, *Phys. Rev. Materials* **3**, 094409 (2019).

[25] X. Zhou, J.-P. Hanke, W. Feng, F. Li, G.-Y. Guo, Y. Yao, S. Blügel, and Y. Mokrousov, Spin-order dependent anomalous Hall effect and magneto-optical effect in the noncollinear antiferromagnets Mn_3XN with $X = Ga, Zn, Ag$, or Ni , *Phys. Rev. B* **99**, 104428 (2019).

[26] K. Zhao, T. Hajiri, H. Chen, R. Miki, H. Asano, and P. Gegenwart, Anomalous Hall effect in the noncollinear antiferromagnetic antiperovskite $Mn_3Ni_{1-x}Cu_xN$, *Phys. Rev. B* **100**, 045109 (2019).

[27] V. T. N. Huyen, M.-T. Suzuki, K. Yamauchi, and T. Oguchi, Topology analysis for anomalous Hall effect in the noncollinear antiferromagnetic states of Mn_3AN ($A = Ni, Cu, Zn, Ga, Ge, Pd, In, Sn, Ir, Pt$), *Phys. Rev. B* **100**, 094426 (2019).

[28] Y. You, H. Bai, X. Chen, Y. Zhou, X. Zhou, F. Pan, and C. Song, Room temperature anomalous Hall effect in antiferromagnetic Mn_3SnN films, *Appl. Phys. Lett.* **117**, 222404 (2020).

[29] X. Li, A. H. MacDonald, and H. Chen, Quantum anomalous Hall effect through canted antiferromagnetism, *arXiv:1902.10650* (2019).

[30] N. J. Ghimire, A. S. Botana, J. S. Jiang, J. Zhang, Y.-S. Chen, and J. F. Mitchell, Large anomalous Hall effect in the

chiral-lattice antiferromagnet CoNb_3S_6 , *Nat. Commun.* **9**, 3280 (2018).

[31] D. -F. Shao, J. Ding, G. Gurung, S.-H. Zhang, and E. Y. Tsymbal, Interfacial Crystal Hall Effect Reversible by Ferroelectric Polarization, *Phys. Rev. Applied* **15**, 024057 (2021).

[32] K. Samanta, M. Ležaić, M. Merte, F. Freimuth, S. Blügel, and Y. Mokrousov, Crystal Hall and crystal magneto-optical effect in thin films of SrRuO_3 , *J. Appl. Phys.* **127**, 213904 (2020).

[33] J. Kipp, K. Samanta, F. R. Lux, M. Merte, D. Go, J.-P. Hanke, M. Redies, F. Freimuth, S. Blügel, M. Ležaić, and Y. Mokrousov, The chiral Hall effect in canted ferromagnets and antiferromagnets, *Commun. Phys.* **4**, 99 (2021).

[34] S. Hayami, Y. Yanagi, and H. Kusunose, Momentum-dependent spin splitting by collinear antiferromagnetic ordering, *J. Phys. Soc. Jpn.* **88**, 123702 (2019).

[35] L.-D. Yuan, Z. Wang, J. -W. Luo, E. I. Rashba, and A. Zunger, Giant momentum-dependent spin splitting in centrosymmetric low-Z antiferromagnets, *Phys. Rev. B* **102**, 014422 (2020).

[36] L.-D. Yuan, Z. Wang, J. -W. Luo, and A. Zunger, Prediction of low-Z collinear and noncollinear antiferromagnetic compounds having momentum-dependent spin splitting even without spin-orbit coupling, *Phys. Rev. Materials* **5**, 014409 (2021).

[37] J. Železný, Y. Zhang, C. Felser, and B. Yan, Spin-Polarized Current in Noncollinear Antiferromagnets, *Phys. Rev. Lett.* **119**, 187204 (2017).

[38] M. Kimata, H. Chem, K. Kondou, S. Sugimoto, P. K. Muduli, M. Ikhlas, Y. Omori, T. Tomita, A. H. MacDonald, S. Nakatsuji, and Y. Otani, Magnetic and magnetic inverse spin Hall effects in a non-collinear antiferromagnet, *Nature (London)* **565**, 627 (2019).

[39] A. Mook, R. R. Neumann, A. Johansson, J. Henk, and I. Mertig, Origin of the magnetic spin Hall effect: spin current vorticity in the Fermi sea, *Phys. Rev. Research* **2**, 023065 (2020).

[40] R. González-Hernández, L. Šmejkal, K. Výborný, Y. Yahagi, J. Sinova, T. Jungwirth, and J. Železný, Efficient Electrical Spin-Splitter Based on Non-Relativistic Collinear Antiferromagnetism, *Phys. Rev. Lett.* **126**, 127701 (2021).

[41] M. Naka, S. Hayami, H. Kusunose, Y. Yanagi, Y. Motome, and H. Seo, Spin current generation in organic antiferromagnets, *Nat. Commun.* **10**, 4305 (2019).

[42] H. Y. Ma, M. Hu, N. Li, J. Liu, W. Yao, J.-F. Jia, and J. Liu, Multifunctional antiferromagnetic materials with giant piezomagnetism and noncollinear spin current, *Nat. Commun.* **12**, 2846 (2021).

[43] D.-F. Shao, S. H. Zhang, M. Li, C. B. Eom, and E. Y. Tsymbal, Spin-neutral currents for spintronics, *Nat. Commun.* **12**, 7061 (2021).

[44] S. Hu, D. -F. Shao, H. Yang, M. Tang, Y. Yang, W. Fan, S. Zhou, E. Y. Tsymbal, and X. Qiu, Efficient field-free perpendicular magnetization switching by a magnetic spin Hall effect, *arXiv:2103.09011* (2021).

[45] L. Šmejkal, A. B. Hellenes, R. G. Hernández, J. Sinova, and T. Jungwirth, Giant and tunneling magnetoresistance effects from anisotropic and valley-dependent spin-momentum interactions in antiferromagnets, *arXiv:2103.12664* (2021).

[46] D. Fruchart and E. F. Bertaut, Magnetic studies of the metallic perovskite-type compounds of manganese, *J. Phys. Soc. Jpn.* **44**, 781 (1978).

[47] K. Takenaka, M. Ichigo, T. Hamada, A. Ozawa, T. Shibayama, T. Inagaki, and K. Asano, Magnetovolume effects in manganese nitrides with antiperovskite structure, *Sci. Technol. Adv. Mater.* **15**, 015009 (2014).

[48] C. X. Quintela, K. Song, D. -F. Shao, L. Xie, T. Nan, T. R. Paudel, N. Campbell, X. Pan, T. Tybell, M. S. Rzchowski, E. Y. Tsymbal, S. Y. Choi, and C. B. Eom, Epitaxial antiperovskite/perovskite heterostructures for materials design, *Sci. Adv.* **6**, eaba4017 (2020).

[49] See Supplemental Material at <http://link.aps.org/supplemental/10.1103/PhysRevMaterials.5.124411> for the description of calculation methods, magnetic ground state of antiperovskites ANMn_3 , and \hat{T} -odd and even charge-to-spin conversion efficiency, which includes Refs. [50–64].

[50] P. Giannozzi, S. Baroni, N. Bonini, M. Calandra, R. Car, C. Cavazzoni, D. Ceresoli, G. L. Chiarotti, M. Cococcioni, I. Dabo, A. Dal Corso, S. de Gironcoli, S. Fabris, G. Fratesi, R. Gebauer, U. Gerstmann, C. Gougoussis, A. Kokalj, M. Lazzeri, L. Martin-Samos *et al.*, QUANTUM ESPRESSO: a modular and open-source software project for quantum simulations of materials, *J. Phys.: Condens. Matter* **21**, 395502 (2009).

[51] D. Vanderbilt, Soft self-consistent pseudopotentials in a generalized eigenvalue formalism, *Phys. Rev. B* **41**, 7892 (1990).

[52] J. P. Perdew, K. Burke, and M. Ernzerhof, Generalized Gradient Approximation Made Simple, *Phys. Rev. Lett.* **77**, 3865 (1996).

[53] J. Železný, Wannier linear response, 2020, <https://bitbucket.org/zeleznyj/wannier-linear-response/wiki/Home>.

[54] N. Marzari, A. A. Mostofi, J. R. Yates, I. Souza, and D. Vanderbilt, Maximally localized Wannier functions: theory and applications, *Rev. Mod. Phys.* **84**, 1419 (2012).

[55] G. Pizzi, V. Vitale, R. Arita, S. Blügel, F. Freimuth, G. Géranton, M. Gibertini, D. Gresch, C. Johnson, T. Koretsune, J. Ibañez-Azpiroz, H. Lee, J.-M. Lihm, D. Marchand, A. Marrazzo, Y. Mokrousov, J. I. Mustafa, Y. Nohara, Y. Nomura, L. Paulatto *et al.*, WANNIER90 as a community code: new features and applications, *J. Phys.: Condens. Matter* **32**, 165902 (2020).

[56] J. Železný, Linear response symmetry, <https://bitbucket.org/zeleznyj/linear-response-symmetry> (2020).

[57] K. Momma and F. Izumi, VESTA: a three-dimensional visualization system for electronic and structural analysis, *J. Appl. Crystal.* **41**, 653 (2008).

[58] M. Kawamura, FERMISURFER: Fermi-surface viewer providing multiple representation schemes, *Comput. Phys. Commun.* **239**, 197 (2019).

[59] E. F. Bertaut, D. Fruchart, J. P. Bouchaud, and R. Fruchart, Diffraction neutronique de Mn_3GaN , *Solid St. Commun.* **6**, 251 (1968).

[60] K. Shi, Y. Sun, J. Yan, S. Deng, L. Wang, H. Wu, P. Hu, H. Lu, M. I. Malik, Q. Huang, and C. Wang, Baromagnetic effect in antiperovskite $\text{Mn}_3\text{Ga}_{0.95}\text{N}_{0.94}$ by neutron powder diffraction analysis, *Adv. Mater.* **28**, 3761 (2016).

[61] P. Lukashev, R. F. Sabirianov, and K. Belashchenko, Theory of piezomagnetic effect in Mn-based antiperovskites, *Phys. Rev. B* **78**, 184414 (2008).

[62] J. Zemen, Z. Gercsi, and K. G. Sandeman, Piezomagnetism as a counterpart of the magnetovolume effect in magnetically frustrated Mn-based antiperovskite nitrides, *Phys. Rev. B* **96**, 024451 (2017).

[63] D.-F. Shao, G. Gurung, T. R. Paudel, and E. Y. Tsymbal, Electrically reversible magnetization at the antiperovskite/perovskite interface, *Phys. Rev. Materials* **3**, 024405 (2019).

[64] H. K. Singh, I. Samathrakis, N. M. Fortunato, J. Zemen, C. Shen, O. Gutfleisch, and H. Zhang, Multifunctional antiperovskites driven by strong magnetostructural coupling, *npj Comput. Mater.* **7**, 98 (2021).

[65] D. Matsunami, A. Fujita, K. Takenaka, and M. Kano, Giant barocaloric effect enhanced by the frustration of the antiferromagnetic phase in Mn_3GaN , *Nat. Mater.* **14**, 73 (2015).

[66] D. Boldrin, A. P. Mihai, B. Zou, J. Zemen, R. Thompson, E. Ware, B. V. Neamtu, L. Ghivelder, B. Esser, D. W. McComb, P. Petrov, and L. F. Cohen, Giant piezomagnetism in Mn_3NiN , *ACS Appl. Mater. & Int.* **10**, 18863 (2018).

[67] P. Lukashev, K. D. Belashchenko, and R. F. Sabirianov, Large magnetoelectric effect in ferroelectric/piezomagnetic heterostructures, *Phys. Rev. B* **84**, 134420 (2011).

[68] G. Gurung, D. -F. Shao, and E. Y. Tsymbal, Spin-torque switching of noncollinear antiferromagnetic antiperovskites, *Phys. Rev. B* **101**, 140405(R) (2020).

[69] R. J. Soulen, Jr., J. M. Byers, M. S. Osofsky, B. Nadgorny, T. Ambrose, S. F. Cheng, P. R. Broussard, C. T. Tanaka, J. Nowak, J. S. Moodera, A. Barry, and J. M. D. Coey, Measuring the spin polarization of a metal with a superconducting point contact, *Science* **282**, 85 (1998).

[70] S. K. Upadhyay, A. Palanisami, R. N. Louie, and R. A. Buhrman, Probing Ferromagnets with Andreev Reflection, *Phys. Rev. Lett.* **81**, 3247 (1998).

[71] I. I. Mazin, How to Define and Calculate the Degree of Spin Polarization in Ferromagnets, *Phys. Rev. Lett.* **83**, 1427 (1999).

[72] X. Tao, Q. Liu, B. Miao, R. Yu, Z. Feng, L. Sun, B. You, J. Du, K. Chen, S. Zhang, L. Zhang, Z. Yuan, D. Wu, and H. Ding, Self-consistent determination of spin Hall angle and spin diffusion length in Pt and Pd: the role of the interface spin loss, *Sci. Adv.* **4**, eaat1670 (2018).

[73] A. J. Berger, E. R. J. Edwards, H. T. Nembach, O. Karis, M. Weiler, and T. J. Silva, Determination of the spin Hall effect and the spin diffusion length of Pt from self-consistent fitting of damping enhancement and inverse spin-orbit torque measurements, *Phys. Rev. B* **98**, 024402 (2018).

[74] S. Keller, L. Mihalceanu, M. R. Schweizer, P. Lang, B. Heinz, M. Geilen, T. Brächer, P. Pirro, T. Meyer, and A. Conca, Determination of the spin Hall angle in single-crystalline Pt films from spin pumping experiments, *New J. Phys.* **20**, 053002 (2018).

[75] H. V. Gomonay and V. M. Loktev, Spin transfer and current-induced switching in antiferromagnets, *Phys. Rev. B* **81**, 144427 (2010).

[76] H. Fujita, Field-free, spin-current control of magnetization in non-collinear chiral antiferromagnets, *Phys. Stat. Solidi RRL* **11**, 1600360 (2017).

[77] Y. Yamane, O. Gomonay, and J. Sinova, Dynamics of non-collinear antiferromagnetic textures driven by spin current injection, *Phys. Rev. B* **100**, 054415 (2019).

[78] M.-A. Leroy, A. M. Bataille, F. Bertran, P. Le Fèvre, A. Taleb-Ibrahimi, and S. Andrieu, Electronic structure of the Cr(001) surface and Cr/MgO interface, *Phys. Rev. B* **88**, 205134 (2013).

[79] M.-A. Leroy, A. M. Bataille, B. Dkhil, F. Porcher, A. Barbier, V. L. R. Jacques, Y. Lu, C. Bellouard, T. Hauet, S. Ravy, J. H.-Martin, C. Gatel, K. Bouzehouane, A. Gukasov, S. Andrieu, and C. Tiusan, Tunnel-mediated coupling between antiferromagnetic thin films, *Phys. Rev. B* **90**, 035432 (2014).